Journal of Manufacturing and Materials Processing

MDPI

Article

Assessing electrode characteristics in continuous resistance spot welding of BH 340 steel based on dynamic resistance

Dawei Zhao[1]*, Nikita Vdonin[1], Mikhail Slobodyan[2], Sergey Butsykin[3], Alexey Kiselev[3] and Anton Gordynets[3]

[1]Department of Welding Engineering, South Ural State University, Chelyabinsk 454080, Russia
[2]Tomsk Scientific Center of the Siberian Branch of the Russian Academy of Sciences, 10/4 Academichesky Avenue, Tomsk, 634055, Russia
[3]School of Advanced Manufacturing Technologies, Tomsk Polytechnic University, Tomsk, 634050, Russia
* Correspondence: Corresponding author: zhaodawei0322@xy.hfut.edu.cn (Dawei Zhao).

Abstract: The aim of this investigation is to offer a data-based scheme for predicting electrode wear in resistance spot welding. One of the major factors affecting the mechanical properties of spot welds and the variation in weld quality is electrode wear and alloying. In this study, Rogowski coils and twisted pairs attached to the top and bottom electrodes were used to obtain the welding current and the voltage between the electrodes in the welding process, thereby calculating the dynamic resistance value during the welding process. The electrode diameter was obtained from the pressure exerted by the upper and lower electrodes on the carbon paper when the current was cut off and was regarded as an indicator of electrode wear. By continuously welding 0.5mm thick BH 340 steel plates until the electrode failed, the dynamic resistance signal was recorded in real time. Simultaneously, the electrode diameter after every 4 welds was also recorded. On this basis, the correlation between electrode diameter and dynamic resistance is studied. In order to quantitatively study the mapping relationship between dynamic resistance and electrode wear, 11 characteristic values were extracted from the dynamic resistance, and the stepwise regression method was used to obtain the regression formula between the characteristic values and the electrode diameter. Using new data to verify the effectiveness of the regression model, the acquired results display that the maximum error between the predicted value of the electrode diameter and the measured value obtained by the regression equation with the interactive quadratic term is 0.3 mm, and the corresponding relative error is 7.69 %. This result demonstrates that the method proposed in this paper can effectively monitor the electrode wear and failure process.

Keywords: resistance spot welding; electrode wear; dynamic resistance; failure process; electrode life

Citation: Zhao, D.; Vdonin, N.; Slobodyan, M.; Butsykin, S.; Kiselev, A.; Gordynets, A. Assessing electrode characteristics in continuous resistance spot welding of BH 340 steel based on dynamic resistance. *J. Manuf. Mater. Process.* **2023**, *6*, x. https://doi.org/10.3390/xxxxx

Academic Editor(s):

Received: date
Revised: date
Accepted: date
Published: date

1. Introduction

In recent years, coated steel plate has been used in many industries because coatings can greatly improve the corrosion resistance of steel products [1]. Galvanised steel is the most common form of coated steel, with usage increasing substantially. In car manufacturing, the use of zinc-coated steel sheet can prolong the life of the car body and improve its corrosion resistance. The most common joining technologies in the manufacturing process of the galvanised steel car body are friction stir welding, tungsten inert gas shielded arc welding, laser welding, metal inert gas shielded arc welding and self-piercing riveting, etc [2]. Among them, resistance spot welding is the most frequently used because it has a high degree of automation suitable for large-scale mass production, simple operation and cost saving [3].

The resistance spot welding process and the effect on electrode wear are completely different between galvanised and uncoated steel sheets [4]. Since the presence of the galvanised layer reduces the density of the welding current and increases the conductivity of the steel sheet compared to the uncoated steel sheet, when the same welding process parameters are used to weld the galvanised steel sheet, the welding heat is obviously insufficient. It is therefore necessary to apply a higher welding current. The relatively high welding current and the electrode are prone to metallurgical reactions with the galvanised layer. In addition, the electrode is hot and electrode wear is the major cause of electrode failure during alloying. Yet, in actual production of car body welding, continuous welding is commonly used to enhance welding production efficiency, which accelerates electrode degradation. Studies have exposed that the size of the electrode tip can be a measure of the degree of electrode wear [5]. Then, after hundreds of welds, the electrode tip dimensions must be evaluated to determine the degree of degradation [6].

By producing 400 consecutive welds of galvanised TRIP steel, Mahmud et al. [7] explored the effect of electrode degradation on one such defect, Zn-enhanced liquid metal embrittlement (LME) cracking, in resistance spot welding. The main factor influencing LME cracking was confirmed to be geometric degradation, specifically the radius of curvature. Metallurgical degradation had no effect on LME cracking in the first 200 welds as its influence was overcome by geometrical degradation. Electrode deterioration in continuously welded baked hardening (BH) 220 steel was analysed by Zhao et al [8]. They tested electrode life and weldability by measuring geometric features, analysing mechanical properties and checking the electrode diameter at 88 or 176 weld intervals. Li et al. [9] investigated the mechanical properties, nugget formation and electrode deterioration during continuous welding of aluminium alloy using a Newton Ring electrode and compared it to a typical spherical electrode. Welding quality is found to be more consistent with the improved electrodes and electrode life is also increased. Enrique et al. [10] studied electrode degradation and how it influenced the mechanical properties of welded steel nuts and high-strength steel plates during the resistance projection welding. The above-mentioned studies are mainly focused on the electrode failure process and how it affected welding quality. Nowadays, the methods of artificial intelligence have been applied in many fields. Some researchers have also tried to find the correlations between the electrode failure process and some features extruded from the dynamic signals in the welding process. Panza et al. [11] indirectly monitored electrode degradation during welding by analysing the electrode displacement signal from a contactless sensor embedded in the welder and electrode tip shape from carbon impression tests. The established model showed good accuracy. The mean error of the contact area was about 1.61 mm^2 and the standard deviation was about 3.73 mm^2.

Since coated hot-rolled steel has good corrosion resistance, it is commonly used in automobile bodies, automobile engines, railway transportation, oil pipelines, bridges and other fields. The most outstanding representative is galvanised bake-hardened (BH) steel, which has excellent corrosion resistance, decent mechanical properties and ductility, and has become one of the most widely used materials in car bodies [12]. Since the steel sheet has been heat treated in an oven at 200 degrees Celsius for about 20 minutes, its strength, toughness and weldability have been improved. Nevertheless, Welding of zinc-coated BH steel has a number of unique difficulties, and it is not possible to copy welding parameters from other ordinary steels. That's because the coating has completely different physical and mechanical properties to the parent metal. Therefore, although the coating improves the corrosion resistance of the steel plate, it has a negative effect on the welding of the steel plate. During resistance spot welding, the presence of the coating acts as an unwanted shunt, requiring a higher welding current and electrode pressure [13]. However, the choice of these welding parameters increases the likelihood of welding defects such as expulsion and cracks. In addition, the coating reacts readily with the electrode at high temperatures, causing wear and alloying of the electrode, thereby reducing the life of the electrode.

BH steel plates are widely used in car bodies. Research has also been published on the welding characteristics of BH steel plates [14-15]. The degree of electrode wear has a non-negligible effect on the strength of resistance spot welded joints of BH steel plates. The dynamic resistance is a key signal in resistance spot welding and is closely related to weld quality. However, research into the relationship between the dynamic resistance signal and spot-welding electrode wear is still at a preliminary stage, and relevant quantitative research is even rarer. In this study, resistance spot welding experiments were carried out on 0.5 mm thick BH 340 steel plates until the electrode failed. At the same time, dynamic resistance signals and electrode diameter changes are collected. In addition, the evolution of the dynamic resistance with electrode wear will be studied and models to predict electrode wear will be developed. In this way, the purpose of monitoring electrode wear through the dynamic resistance signal during the continuous welding process is achieved.

2. Experimental procedure

2.1. Experimental materials and welding conditions

BH340 galvanised steel plate, 0.5mm thick, is used as the welding material in the welding experiment. Table 1 provides the chemical composition and mechanical properties of the steel plate and the composition of the coating.

Table 1. Chemical compositions and mechanical attributes of BH 340 and the coating (%).

Chemical compositions							Mechanical properties			Zn coating		
C	Si	Mn	P	S	Al	Cu	Rel (MPa)	Rm (MPa)	A80 (%)	Elongation/A80 (%)	Thickness/t (μm)	Mass/m (g/m2)
0.025	0.03	0.44	0.009	0.015	0.044	⩽0.2	360	425	28	41	15	200

R_{el} yield strength, R_m ultimate tensile strength, $A80$ elongation

The medium frequency direct current (MFDC) resistance spot welding machine is used to weld steel plates [16], and the welding mode is constant current mode. In order to reduce the effect of stains on the surface of the steel plate upon the welding quality, the steel plate must be mechanically and chemically cleaned before welding. First of all, the steel plate should be wiped several times with industrial alcohol, then rubbed with a clean, damp cloth, and left to dry in a well-ventilated place. As the thickness of the steel plate is extremely small, the post-weld cooling method is air cooling. The end diameter of the electrode is 3 mm and its material is Cu-Cr alloy. Figure 1 shows the electrode dimensions in detail.

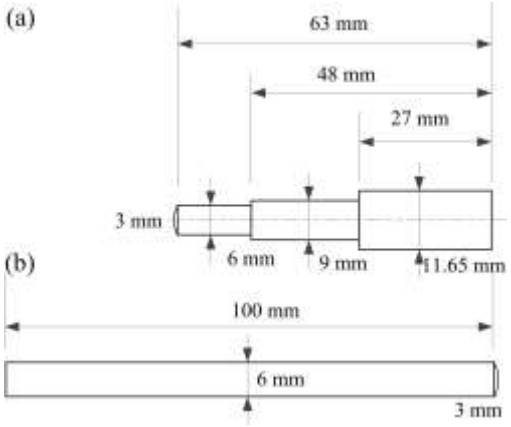

Figure 1. Geometry of the electrodes: (a) the upper electrode; (b) the lower electrode.

In order to inspect electrode wear, it is essential to select appropriate spot-welding process parameters and repeat the welding operations. When implementing continuous

welding on two large stacked steel plates, certain measures must be taken to reduce the adverse effect on the weld quality caused by welding current shunting. In actual operation, the distance between the welding points and the edge of the welding plate is set at 20 mm in order to save the consumption of welded steel plates and to minimise the effect of current shunt on the welding quality. Figure 2 shows the layout of the welding points. The welding current during the welding process is 4.0 kA, which is slightly lower than the critical welding current when spatter occurs to ensure weld quality. The other welding process parameters are listed in Table 2. The specific waveform of the welding current is shown in Figure 3.

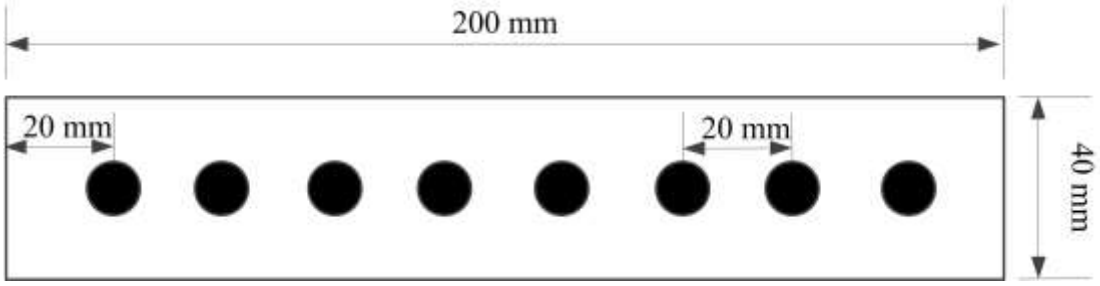

Figure 2. Distances between edges and welds on the plates.

Table 2. Schematisation of the spot weld schedule used in the experimental runs.

Welding current	Welding time	Hold time	Electrode force
4 kA	60 ms	10 ms	360 N

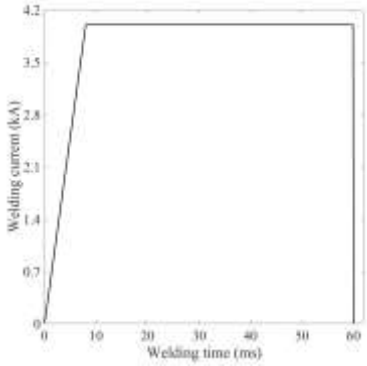

Figure 3. The welding current waveform.

For continuous spot welding, dynamic resistance signals are recorded in real time. Figure 4 shows the test system for measuring current and voltage during welding. The Rogowski coil is employed to measure the welding current value during the welding process, while the voltage between the top and bottom electrodes is simply obtained using the alligator clip cable. The acquired signal must be converted from analogue to digital and input to the oscilloscope for display. The signal can be output via the oscilloscope's USB interface and copied to the computer for further processing.

Figure 4. The measurement system of the dynamic resistance.

During continuous welding, use carbon paper to record the changes in diameter of the electrode tip after every 4 welding points. When using carbon paper to record the geometric dimensions of the electrode tip, use the same welding process parameters as for actual welding, except that the welding current must be turned off at this time. The resulting electrode indentation was then placed under a low power magnifying glass and its geometric dimensions measured. Figure 5 shows the electrode diameter when welding 20 points.

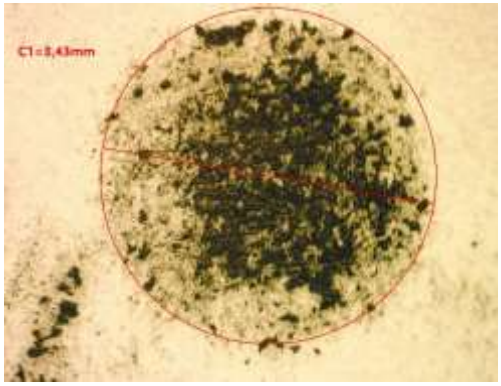

Figure 5. The measurement of the electrode diameter for the 20th weld.

3. Experimental results and discussion

3.1. Dynamic resistance signal characteristics

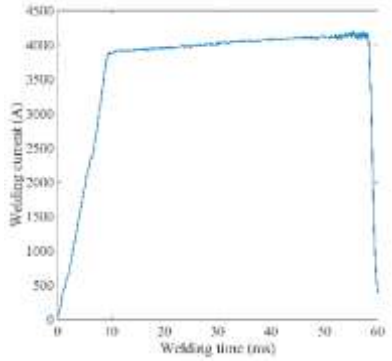

Figure 6. The measured welding current for the 20th weld.

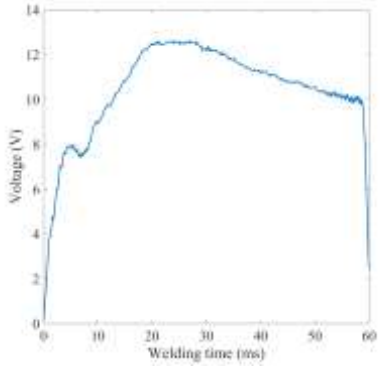

Figure 7. The measured voltage for the 20th weld.

Figures 6 and 7 show the inter-electrode voltage and welding current signals as the 20th weld point is welded. At this time, the corresponding welding current is 4 kA, the welding time is 60 ms and the electrode pressure is 360 N. A medium frequency direct current resistance spot welding machine is utilised for this purpose. This ensures that the current variation during the welding process is very small, in contrast to the alternating current spot welder. Therefore, the dynamic resistance signal during the welding process can be obtained directly from Ohm's law.

$$R(t)=U(t)/I(t) \quad (1)$$

where $R(t)$ is the dynamic resistance, $U(t)$ is the voltage, I (t) is the welding current and t is the welding time.

Figure 8 shows the dynamic resistance signal of the 20th weld. In general, the change in dynamic resistance with welding time can be divided into three stages. First, the welding current gradually increases from a very low value to 4kA and stabilises at this value. The upper and lower welding plates generate contact resistance affected by electrode pressure. The contact resistance generates heat and causes the contact surface of the welding plate to soften when exposed to the welding current. The contact area of the upper and lower steel plates increases, the contact resistance decreases and the dynamic resistance value decreases until it reaches the α point. After the upper and lower metal plates are in close contact, the temperature of the welded area increases under the effect of resistance heat. As a result, the resistivity of the BH 340 steel plate increases and when the temperature reaches the melting point of the metal, the metal melts. At this stage, the dynamic resistance increases until it reaches the β point. This point means that the metal in the weld area has melted to a certain extent and the liquid nugget has reached a certain size. Next, the energy dissipated by the electrode exceeds the heat created by the welding current and the dynamic resistance decreases again until it reaches the end point.

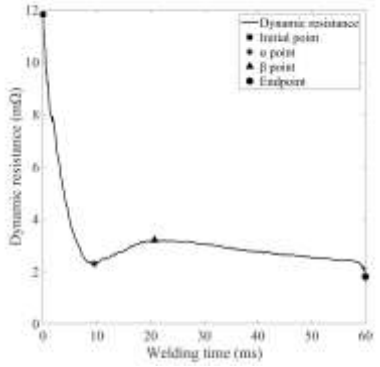

Figure 8. A typical dynamic resistance signal.

The basic objective of this study is to construct a robust model to quantitatively approximate the true functional relationship between the dynamic resistance signal and the electrode end diameter in the non-stop resistance spot welding process, focusing on the mapping relationship between the dynamic resistance signal and the electrode end diameter. Therefore, it is very necessary to first correlate the dynamic resistance curve with the electrode diameter. However, a dynamic resistance curve contains hundreds of data, so it is necessary to extract the most important data to achieve dimensionality reduction. Figure 9 shows the evolution of the dynamic resistance signal when repeated at different welding times. The figure clearly shows that the dynamic resistance signal changes regularly as the number of joints increases. The resistance value at the β point gradually decreases and the welding time to reach this value is delayed accordingly. The overall dynamic resistance curve shows a downward trend as the number of joints increases, which is caused by the increasing electrode end diameter due to electrode wear and the resulting decrease in welding current density [17]. This finding is consistent with previous research showing that an increase in electrode tip diameter is an indication of electrode wear [18]. When electrode wear is severe, the welding current density will decrease and the resulting heat will also decrease. At this point, the heating rate of the weld area is slower and it takes longer to reach the same welding heat as the previous weld point, so the time for the corresponding key points to appear is also delayed. The same conclusion can be drawn from Ohm's law, welding heat is in direct proportion to the square of the welding current. If the density of the welding current is lower, it takes longer to reach a given welding heat. Bogaerts et al. [19] discovered that the time to reach the β-point of the dynamic resistance is highly related to the heating rate during welding. It can be realised that the resistance value of the β point is also closely related to the corresponding welding time and the degree of electrode wear.

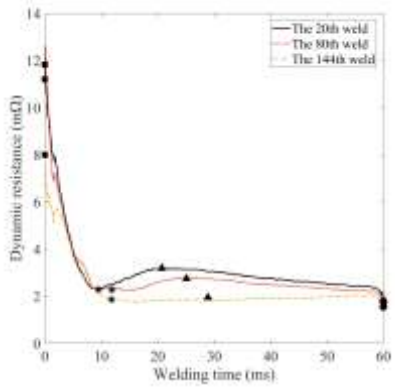

Figure 9. Dynamic resistance variation during electrode failure.

According to the change of dynamic resistance with the number of solder joints, some feature points can be extracted from the signal to express its changes. The positions of the α and β points and their resistance values are extracted. The final value of the resistance signal [20] and the integral value of the dynamic resistance [21] are also extracted. The slope between the four key points of the dynamic resistance (start point, α point, β point and end point) is also calculated. Table 3 lists the 11 feature values extracted from the dynamic resistance signal. Their statistical values are shown in Table 4.

Table 3. Interpretation of the extracted characteristics of the dynamic resistance signal.

Characteristics	Equation	Unit	Definition
r_0	-	mΩ	The resistance of the initial point.
t_α	-	ms	The position of the α point.

r_α	-	mΩ	The resistance of the α point.
t_β	-	ms	The position of the β point.
r_β	-	mΩ	The resistance of the β point.
r_e	-	mΩ	The resistance of the end point.
P	$p = \int r(t)dt$	mΩ·ms	The integration of dynamic resistance.
L	$L = \sum r(t) \times t$	mΩ·ms	The length of dynamic resistance.
k_1	$k_1 = \frac{r_0 - r_\alpha}{t_\alpha}$	Ω/s	The decreasing speed between the initial point and the α point.
k_2	$k_2 = \frac{r_\beta - r_\alpha}{t_\beta - t_\alpha}$	Ω/s	The increasing speed between the α point and the β point.
k_3	$k_3 = \frac{r_\beta - r_e}{60 - t_\beta}$	Ω/s	The decreasing speed between the β point and the end point.

Table 4. The statistical characteristics of the extracted features of all dynamic resistance signals and electrode diameter.

Characteristics	Unit	Minimum	Maximum	Mean	Median	Mode	Standard error	Range
r_0	mΩ	5.333	22.4	11.74	10.67	10.4	4.106	17.07
t_α	ms	8.11	15	11.36	10.55	9.548	1.923	6.89
r_α	mΩ	1.457	3.137	2.331	2.394	1.457	0.4135	1.68
t_β	ms	13.02	43.27	24.16	22.71	20.5	6.337	30.25
r_β	mΩ	1.666	3.601	2.898	3.089	1.666	0.4856	1.935
r_e	mΩ	1.291	1.991	1.784	1.803	1.969	0.1847	0.7002
P	mΩ·ms	110	202.2	175.9	186.1	110	24.36	92.14
L	mΩ·ms	63.37	80.58	68.29	67.27	63.37	3.827	17.21
k_1	Ω/s	0.2684	1.943	0.8618	0.7756	0.2684	0.4278	1.675
k_2	Ω/s	0.006496	0.1752	0.05352	0.04875	0.006496	0.03701	0.1687
k_3	Ω/s	0.009177	0.04564	0.03008	0.03058	0.009177	0.007993	0.03647
D	mm	2.88	3.98	3.619	3.66	3.64	0.2652	1.1

3.2. Establishing models for the extracted features

Regression analysis, a quantitative statistical/computational technique, examines the functional relationship between independent variables and dependent variables in order to simulate and approximate the mapping relationship between them to the maximum extent. The regression model is obtained by analysing the relationship between the independent variables and the dependent variables using the method of least squares. Analysis of variance (ANOVA) was used as a tool to determine the significance and robustness of the regression model.

Assuming the independent variables ($X_1, X_2, \cdots X_n$) are continuous, their errors are small enough to be ignored. The functional relationship between the independent variable ($X_1, X_2, \cdots X_n$) and the dependent variable y can be given by the following formula [22]:

$$y = f(x_1, x_2, \cdots x_n) \quad (2)$$

The functional relationship between independent and dependent variables requires a more accurate approximation. It is thus necessary to establish a non-linear regression equation to simulate the mapping relationship between them. The polynomial regression model is the most commonly used and its expression can usually be described as follows:

$$f(x_1, x_2, \cdots x_n) = a_0 + \sum_{i=1}^{n} a_i x_i + \sum_{i=1, j=1}^{n} a_{ij} x_i x_j + \varepsilon \quad (3)$$

Where ε denotes the model error, x_i represents each independent variable, $f(x_1, x_2, \cdots x_n)$ indicates the dependent variable. The regression coefficient a_i can be estimated from the obtained experimental data using the least squares regression method.

To investigate how the characteristics extracted from the dynamic resistance signal correlate with electrode size D, Table 5 expresses the correlation coefficient between them. The table clearly shows that the feature k_3 has the largest correlation coefficient with the electrode diameter of 0.882, while the length L of the dynamic resistance has the smallest correlation coefficient value. Eigenvalues with correlation coefficients less than 0.5 were discarded and the remaining eigenvalues were used as input to the upcoming regression model to predict the electrode diameter. The regression model was obtained using the stepwise regression analysis method and was obtained using MATLAB2017 software. If the P-value of the model and the terms included in the model are less than 0.1, it indicates that they are significant and should be retained. Otherwise, they should be discarded. By calculating the coefficient R^2, the adjusted R^2 and the sum of squared prediction errors, the fit of the regression model can be evaluated. A good regression model should have a coefficient of determination close to 1 and a small sum of squared prediction errors. The data obtained from the welding experiment and the carbon printing experiment on carbon paper are divided into two groups: training samples and test samples. To obtain the regression model, 33 groups of all data were randomly selected as training samples, and another 10 groups of the test samples were used to verify the simulation accuracy and performance of the model.

Table 5. The correlation coefficients between the extracted features and the electrode diameter.

Extracted features	r_0	t_α	r_α	t_β	r_β	r_e	P	L	k_1	k_2	k_3	D
Correlation coefficients	-0.573	0.513	-0.597	0.597	-0.730	0.023	-0.639	-0.210	-0.625	-0.585	-0.882	1

In this study, the regression model was constructed using the stepwise regression method based on the features extracted from the dynamic resistance signal. After trial and error, two linear models were selected as the data were randomly selected to build the model. In this case, the Matlab software constructed different models according to the different data randomly selected each time. After many attempts, it was exposed that there were two types of models with different input variables. In order to find the model with a better performance, we built two models and then compared their performance using completely new data.

Tables 6 and 7 show the ANOVA results of the linear regression model. The R^2 coefficient of this model is 0.9000, which implies that 90% of the experimental data agrees with the predicted data. The model only fails to predict the remaining 10% of the data. The adjusted R^2 is 0.8897, which is very adjacent to 0.9000 and also close to 1. Among the P-

values of all the eigenvalues, only x_1, x_6 and x_9 have P-values lower than 0.05, so the conclusion that can be drawn that they are highly significant [23] and should be retained in this linear regression model.

Table 6. The results of the ANOVA for the first model of the linear regression.

Source	Sum of squares	df	Mean square	F value	P value
Model	2.1767	3	0.7256	87.0441	<0.0001
Residual	0.2417	29	0.0083		
Cor total	2.4185	32			
Standard deviation	0.0913	Mean	3.6073		
R-Squared	0.9000	Adjusted R-Squared	0.8897		

Table 7. Linear regression model ANOVA results for each term.

Term	Estimated value	Standard error	T-value	P-value	P value
Constant	4.0292	0.1450	27.7970	<0.0001	<0.0001
x_1	-0.0123	0.0056	-2.1981	0.0361	
x_6	0.0065	0.0014	4.8235	<0.0001	
x_9	-46.4429	3.8793	-11.9720	<0.0001	

To obtain a more accurate prediction model, a non-linear regression model with interaction terms was attempted to approximate the mapping relationship between the characteristic values of the dynamic resistance curve and the electrode diameter. The eigenvalues extracted from the dynamic resistance curve and the interaction terms between them are used as independent variables in the regression model, and the electrode diameter is the dependent variable. The stepwise regression method was used, and Matlab 2017b software was used to construct a nonlinear regression model. The results of the variance analysis of this nonlinear regression model are illustrated in Tables 8 and 9. The nonlinear regression model is very significant as its P-value is much lower than 0.05. R^2 and adjusted R^2 are very similar and close to 1, and their values are higher than those of the linear model. In such a case, the non-linear regression model is more accurate in predicting the electrode diameter. Figure 10 is a good illustration of this point. The graph reflects that the residual error of the non-linear regression model is smaller.

Table 8. Results of the ANOVA for the non-linear regression model.

Source	Sum of squares	df	Mean square	F value	P value
Model	2.3145	4	0.5786	155.8613	<0.0001
Residual	0.1039	28	0.0037		
Cor total	2.4185	32			
Standard deviation	0.0609	Mean	3.6073		
R-Squared	0.9570	Adjusted R-Squared	0.9509		

Table 9. Non-linear regression model ANOVA results for each term.

Term	Estimated value	Standard error	T-value	P-value	P value
Constant	2.7135	0.2366	11.4662	<0.0001	<0.0001
x_1	0.0016	0.0044	0.3715	0.7130	
x_6	0.0128	0.014	9.3516	<0.0001	
x_9	32.4732	13.2098	2.4583	0.0204	
x_1x_9	-0.4262	0.07	-6.0922	<0.0001	

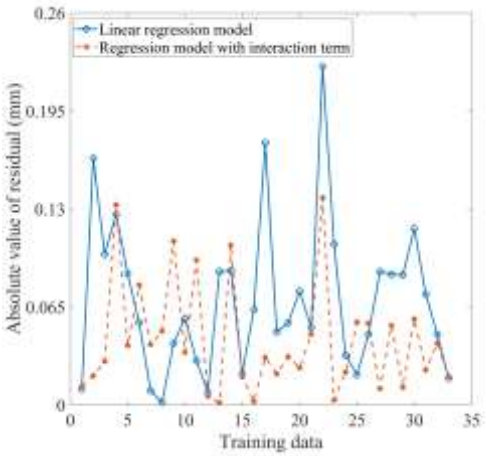

Figure 10. The residuals of the two models based on the training data.

In accordance with the results of the analysis of variance, the two regression models can be depicted as follows:

$$D = 4.0292 - 0.0123x_1 + 0.0065x_6 - 46.4429x_9 \quad (4)$$

$$D = 2.7135 + 0.0016x_1 + 0.0128x_6 + 32.4732x_9 - 0.4262x_1x_9 \quad (5)$$

where D is the electrode diameter, x_1, x_6 and x_9 are the features extracted from the dynamic resistance.

The prediction accuracy of the linear regression model and the non-linear model is shown in Figure 11. This result is obtained using new test data. The maximum prediction error of the non-linear regression model is 0.30 mm, while the maximum prediction error of the linear regression model is 0.50 mm. The corresponding relative prediction errors are 7.69% and 12.75% respectively. It is not difficult to see that the non-linear regression model has a more accurate ability to evaluate and predict the electrode diameter than the linear regression model. In this circumstance, it is highly recommended to use a non-linear regression model related to selected features of the dynamic resistance curve to predict the electrode diameter. Monitoring dynamic resistance signals to obtain changes in electrode diameter can be an effective method of assessing the extent of electrode wear in practical production applications.

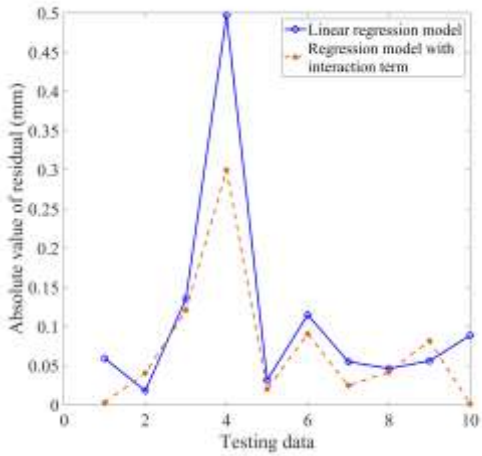

Figure 11. A comparison of the residuals of the two models.

326 **Table 10.** The statistics of the residuals of the two models.

Models	Symbol	Linear regression model	Regression model with interaction terms
Minimum	D_{min}	0.01823	0.001332
Maximum	D_{max}	0.4971	0.2998
Mean	D_{mean}	0.1104	0.0726
Medium	D_{med}	0.05785	0.04148
Standard deviation	σ	0.1406	0.08895
Range	Δ	0.4785	0.2984

327 ## 4. Conclusion

328 (1) As the weld number increases, the β point of the dynamic resistance signal ap-
329 pears later and its value also shows a smaller trend. When the number of welding times
330 increases from 20 to 144, the resistance value of the β point decreases from 3.57 mΩ to 1.84
331 mΩ and its appearance time is delayed by 19.56 ms.

332 (2) The characteristic values extracted from the dynamic resistance curve serve as in-
333 dependent variables, while the electrode diameter is the dependent variable. Based on
334 this, linear and non-linear regression equations are established. The analysis of variance
335 results verify that the P values of the linear regression equation and the non-linear regres-
336 sion equation are both less than 0.0001, and their adjusted R2 values are approximately
337 0.89 and 0.95 respectively.

338 (3) When the prediction accuracy of the regression model was tested using test data,
339 it was found that the non-linear regression model performed better in predicting the elec-
340 trode diameter. Its maximum absolute error is 0.30mm. The maximum relative error is
341 7.69%.

342 (4) Non-linear regression models are considered to be very robust in monitoring elec-
343 trode status. Instead of traditional manual feature extraction methods for predicting elec-
344 trode status, future work may include deep learning methods that process dynamic re-
345 sistance signals and obtain mapping relationships between dynamic resistance signal and
346 electrode wear.

347

348 **Author Contributions:** Dawei Zhao: Conceptualisation, Methodology, Formal analysis, Writing -
349 original draft, Writing - review &editing, Project administration, Funding acquisition. Nikita
350 Vdonin: Software, Data curation. Mikhail Slobodyan: Supervision, Investigation. Sergey Butsykin:
351 Software, Validation, Investigation. Alexey Kiselev: Conceptualisation, Resources, Visualization.
352 Anton Gordynets: Resources, Data curation.

353

354 **Acknowledgements:** For the financial support of the Russian Science Foundation (22-29-20095) the
355 authors of this article are grateful.

356 **Conflicts of Interest:** No author has a conflict of interest with respect to the subject matter of the
357 paper.

358 ## References

359 [1] Schmolke, T.; Brunner-Schwer, C.; Biegler, M.; Rethmeier, M.; Meschut, G. On welding of high-strength steels using laser
360 beam welding and resistance spot weld bonding with emphasis on seam leak tightness. Journal of Manufacturing and Materials
361 Processing 2023, 7(3), 116.
362 [2] Palmieri, M.E.; Galetta, F.R.; Tricarico, L. Study of tailored hot stamping process on advanced high-strength steels. Journal of
363 Manufacturing and Materials Processing 2022, 6(1), 11.
364 [3] Khalil, C.; Marya, S.; Racineux, G. Magnetic pulse welding and spot welding with improved coil efficiency—Application for
365 dissimilar welding of automotive metal alloys. Journal of Manufacturing and Materials Processing 2020, 4(3), 69.
366 [4] Zhao, D., Vdonin, N., Radionova, L., Glebov, L.; Guseinov, K. Resistance spot welding of high-strength low-alloyed (HSLA)
367 420 steel and bake-hardening (BH) 220 steel. The International Journal of Advanced Manufacturing Technology 2023, 128(3-
368 4), 1441-1453.

[5] Bachchhav, B.; Bharne, S.; Choudhari, A.; Pattanshetti, S. Selection of spot welding electrode material by AHP, TOPSIS, and SAW. Materials Today: Proceedings 2023, https://doi.org/10.1016/j.matpr.2023.02.253.
[6] Bachchhav, B.D.; Chaitanya, S.V.; Salunkhe, S.; Chandrakumar, P.; Pagáč, M.; Nasr, E.A. Wear performance of Cu–Cd, Cu–Be and Cu–Cr–Zr spot welding electrode materials. Lubricants 2023, 11(7), 291.
[7] Mahmud, K.; Murugan, S.P.; Cho, Y.; Ji, C.; Nam, D.; Park, Y.D. Geometrical degradation of electrode and liquid metal embrittlement cracking in resistance spot welding. Journal of Manufacturing Processes 2021, 61, 334-348.
[8] Zhao, D.; Vdonin, N.; Bezgans, Y.; Radionova, L.; Glebov, L. Correlating electrode degradation with weldability of galvanized BH 220 steel during the electrode failure process of resistance spot welding. Crystals 2023, 13(1), 39.
[9] Li, M.; Wang, Y.; Yang, S.; Tao, W.; Zhang, G. Improving mechanical properties and electrode life for joining aluminum alloys with innovatively designated Newton ring electrode. Journal of Manufacturing Processes 2021, 64, 948-959.
[10] Enrique, P.D.; Al Momani, H.; DiGiovanni, C.; Jiao, Z.; Chan, K.R.; Zhou, N.Y. Evaluation of electrode degradation and projection weld strength in the joining of steel nuts to galvanized advanced high strength steel. Journal of Manufacturing Science and Engineering 2019, 141(10), 104501.
[11] Panza, L.; De Maddis, M.; Spena, P.R. Use of electrode displacement signals for electrode degradation assessment in resistance spot welding. Journal of Manufacturing Processes 2022, 76, 93-105.
[12] Johnson, N.N.; Madhavadas, V.; Asati, B.; Giri, A.; Hanumant, S.A.; Shajan, N.; Arora, K.S. Multi-objective optimization of resistance spot welding parameters of BH340 steel using Kriging and NSGA-III. Transactions of the Indian Institute of Metals 2023, 76, 3007-3020.
[13] Pawar, S.; Singh, A.K.; Park, K.S.; Choi, S.H. Effect of welding current on the microstructural evolution and lap-shear performance of resistance spot-welded 340BH steel. Materials Characterization 2023, 203, 113126.
[14] Özkul, İ.; Şehirli, S.; Akkurt, A. Effects of laser and electron beam welding on the mechanical properties of bake hardening sheets. Materials Testing 2022, 64(1), 88-97.
[15] Pawar, S.; Singh, A.K.; Kaushik, L.; Park, K.S.; Shim, J.; Choi, S.H. Characterizing local distribution of microstructural features and its correlation with microhardness in resistance spot welded ultra-low-carbon steel: Experimental and finite element characterization. Materials Characterization 2022, 194, 112382.
[16] Butsykin, S.; Gordynets, A.; Kiselev, A.; Slobodyan, M. Evaluation of the reliability of resistance spot welding control via on-line monitoring of dynamic resistance. Journal of Intelligent Manufacturing 2023, 34(7), 3109-3129.
[17] Zhou, L.; Li, T.; Zheng, W.; Zhang, Z.; Lei, Z.; Wu, L.; Zhu, S.; Wang, W. Online monitoring of resistance spot welding electrode wear state based on dynamic resistance. Journal of Intelligent Manufacturing 2022, 33, 91-101.
[18] Martín, Ó.; De Tiedra, P. Advances in the control and improvement of quality in the resistance spot welding Process. Metals 2022, 12(11), 1810.
[19] Bogaerts, L.; Dejans, A.; Faes, M.G.; Moens, D. A machine learning approach for efficient and robust resistance spot welding monitoring. Welding in the World 2023, 67, 1923-1935.
[20] Wen, J.; Jia, H. Real-time monitoring system for resistance spot welding quality. Engineering Research Express 2023, 5(1), 015006.
[21] Chen, G.; Sheng, B.; Luo, R.; Jia, P. A parallel strategy for predicting the quality of welded joints in automotive bodies based on machine learning. Journal of Manufacturing Systems 2022, 62, 636-649.
[22] Xing, L.; Yu, T.; Zhang, J.; Xing, X.; Lu, H. Optimization and improvement of the projection welding of nut based on regression analysis. ISIJ International 2023, 63(4), 694-702.
[23] Anandan, B.; Manikandan, M. Machine learning approach with various regression models for predicting the ultimate tensile strength of the friction stir welded AA 2050-T8 joints by the K-Fold cross-validation method. Materials Today Communications 2023, 34, 105286.